Multi-channel integrated optical filters for spectral signature recognition

Dmitri Iazikov*, Christoph M. Greiner, and Thomas Mossberg
LightSmyth Technologies, Inc, Suite 250, 860 West Park Street, Eugene, OR 97401

ABSTRACT

Recent advances in the development of two-dimensional holographic Bragg reflectors in planar lightwave circuits have demonstrated the feasibility of highly customizable multi-wavelength filters based on photonics nanostructures programmable to recognize spectra with up to 2000 spectral lines. Such filters rival or exceed performance of free space gratings, thin film filters and Bragg gratings and may be monolithically integrated with detectors in III-V active materials or as passive devices in silica. This new technological platform holds a great promise of being next-generation optical engine for spectral signature recognition in the field of remote sensing, biological, chemical and defense applications.

Keywords: holographic Bragg reflectors, spectral filter, planar lightwave circuits, nanophotonics, waveguides.

1. INTRODUCTION.

Remote sensing, material analysis, medicine and biology have been using optical spectral analysis for the detection of chemical elements and biological compounds for many decades. Traditionally, spectral analysis is performed using spectrometers. Nowadays spectrometers are very complex and powerful tools typically involving sophisticated computerized analysis of recorded spectra with the ability to detect hundreds of spectra of interest. Recently a new type of multi-wavelength integrated spectral filter based on technology we refer to as holographic Bragg reflectors (HBR)[1] was introduced and provides an attractive alternative to optical spectrometers.

HBR-based filters are capable of performing real-time analysis of input spectra optically rather than electronically. For example, a reference spectral signature containing hundreds of spectral lines characteristic for a chemical element may be encoded into the optical structure of an HBR. When the spectrum of an input signal contains the reference spectral signatures, it will generate optical signal at the output of HBR with the intensity proportional to the concentration of the chemical element in question. Extremely compact and lightweight, with no moving parts, monolithically integrated HBR filters provide a viable solution for remote sensing of pre-defined chemical and biological agents in aerospace, military and airborne applications.

2. OPERATION PRINCIPLES OF HOLOGRAPHIC BRAGG REFLECTORS.

HBR-based filters are two-dimensional distributed diffractive structures fabricated in planar optical waveguides. HBR's employ state-of-the art deep-ultraviolet (DUV) photolithography and silica-on-silicon planar waveguide processes perfected largely in the context of planar lightwave circuit development[2]. Being true photonic nanostructures, the integrated filters are enabled by advances in the semiconductor industry allowing placement of sub-micron features with an accuracy of 10 nm over the area of hundreds of square mm. The features represent diffractive contours lithographically transferred from a laser-written reticle into the core layer of a slab waveguide, etched into the core using reactive ion etch and filled with material of different refractive index (Fig. 1). The reticle is computer-generated, allowing individual control on the shape of the contours and giving unprecedented flexibility in engineering of the spectral transfer function. The HBR's considered in this paper are formed in standard silica-on-silicon planar waveguides deposited on a silicon substrate and composed of doped SiO_2 (silica) core of one or more sublayers deposited between two 12 to 15 μm thick doped silica cladding layers of lower refractive index. For single-mode operation, typical thickness of the core layer is several micrometers. Alternatively, HBRs may be fabricated in active semiconductor materials allowing monolithic integration with detectors.

* diazikov@lightsmyth.com; www.lightsmyth.com

Instruments, Science, and Methods for Geospace and Planetary Remote Sensing,
edited by Carl A. Nardell, Paul G. Lucey, Jeng-Hwa Yee, James B. Garvin, Proc. of SPIE
Vol. 5660 (SPIE, Bellingham, WA, 2004) · 0277-786X/04/$15 · doi: 10.1117/12.607431

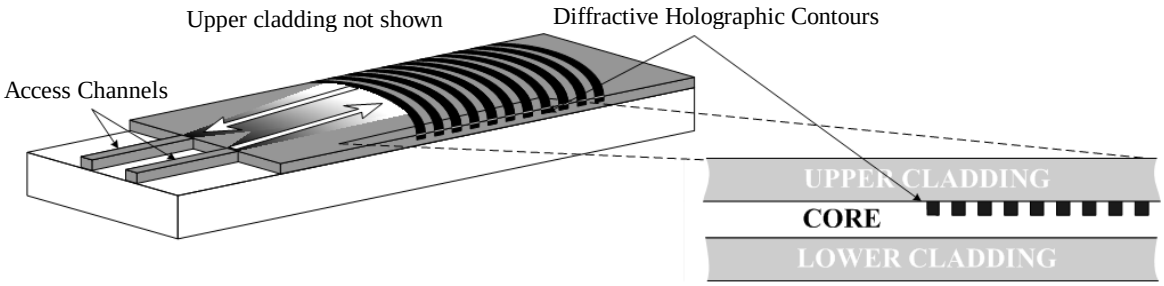

Figure 1: General view (left) and cross-section (right) of holographic Bragg reflector implemented in a planar waveguide. The light enters through an access channel, expands in 2-D planar waveguide and interacts with the diffractive holographic contours lithographically scribed in the waveguide.

Like fiber Bragg gratings [3], the spectral response of an HBR is determined by the interference of light diffracted on the individual contours. The spacing between the diffractive contours and reflective amplitude of each contour determine the spectral transfer function of the filter. There are multiple fabrication-friendly ways to efficiently control the reflective amplitude of the contours. One of them is so-called partial-fill gray scale, when only part of the contour is written so that its reflective amplitude is proportional to the ratio of the written portion to the total length of the contour. In the simple case when the optical path length difference between the successive contours increases by Λ, the nano-structure reflects light at a single resonance wavelength λ defined as $\lambda = 2\, n_{eff}\, \Lambda$, where n_{eff} is the effective refractive index of the waveguide. An HBR typically comprises thousands of diffractive contours. Each contour may be a weak scatterer, but resultant coherent co-operative scattering may easily approach 100% for a specific waveband. The weak scattering properties of HBR diffractive contours allow for much lower propagation loss and polarization dependence compared to conventional photonic crystals. On the other hand, if necessary, HBRs may operate in the high refractive index modulation regime typical of a photonic crystal.

Each diffractive contour also acts as focusing mirror, bringing all imaging capabilities of bulk reflective optics into the plane. Collectively, the contours may be considered as a wavelength-selective mirror imaging input optical signal into the output port. In the examples of devices described further, the diffractive contours have a simple concentric shape with common center of curvature located symmetrically between the input and output optical ports (Fig. 1). Concentric shapes have good imaging properties for small angles between incoming and reflected beams. For larger angles, truly holographic contours (similar to aspherical surfaces in bulk optics) produce optimal imaging. The input and output ports are coupled into access channel waveguides formed on the same chip. The channel waveguides in turn are aligned with butt-coupled optical fibers. In the devices discussed further, single-mode SMF28 fiber was used for testing.

3. MULTI-WAVELENGTH SPECTRAL COMPARATOR.

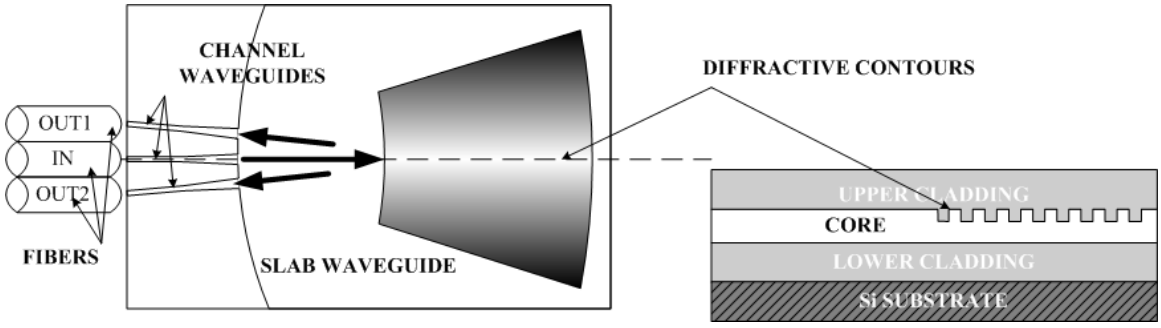

Figure 2. Top view (left) and cross-section (right) of 16-band HBR-based spectral comparator reflecting complementary spectral bands into two output ports.

The strength of HBR-based filters is especially apparent in applications requiring very complex spectral transfer functions. An example of such a device is the 16-band spectral comparator[4] presented in Fig. 2. The device has a common input port and two output ports utilizing channel waveguides to transport signals to the HBR region. The chip size is about 5 x 30 mm. Light from the input channel waveguide is coupled into a slab waveguide containing two HBR's. Each HBR is designed to reflect eight spectral bands separated by approximately 1 nm into a respective output port. Sophisticated amplitude and phase apodization of one of the HBRs is shown in Fig. 3. Amplitude apodization was achieved using partial fill gray scale. Phase apodization was realized by shifting the diffractive contours from uniform spacing by a fraction of wavelength.

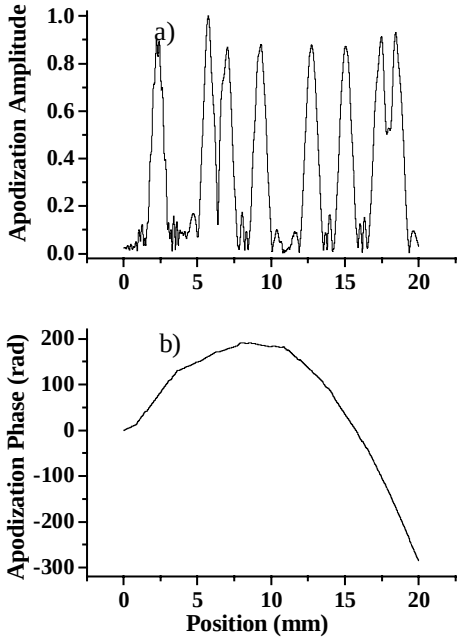

Figure 3. Amplitude (a) and phase (b) apodization of the spectral comparator

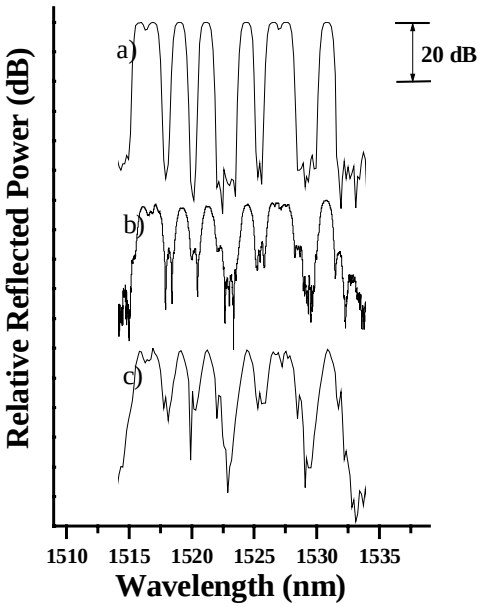

Figure 4. Spectral response of the spectral comparator: (a) initial simulation, (b) measured spectrum, (c) refined simulation taking into account coupling between amplitude apodization and effective refractive index

In spite of the complexity of the device containing about 10 thousand individually apodized contours, it has been reproduced with extremely high fidelity as evident from the comparison of designed and measured spectral performance presented in Fig. 4. At the time of the initial design (Fig. 4a), second-order apodization effect related to coupling between effective refractive index and of the waveguide and degree of the partial fill gray scale was neglected resulting in deviation of the measured spectrum from the initial design (Fig. 4b). When this effect was taken into account, a remarkable correspondence between the simulated and measured spectra was demonstrated (Fig 4c). Such correspondence is an indication that the comparator was very accurately rendered. In future designs, it is possible to compensate for the second-order apodization effect by adjusting the relative position of the contours. Alternatively, other amplitude apodizations techniques that do not affect effective refractive index are feasible and being implemented by the authors.

The spectral comparator served to successfully demonstrate the adequacy of the fabrication process in terms of patterning and etching fidelity and with regards to refractive index uniformity within the planar waveguide layers. It also demonstrated viability of HBR technology for constructing multi-wavelength filters. It was designed for low reflectivity and exhibited minimum fiber-coupled insertion loss of about 8 dB of which fiber-to-waveguide coupling is accounted for 1 dB. No detectable polarization-dependent loss was found, however a polarization-dependent wavelength shift (PDWL) of 0.6 nm was observed corresponding to a fractional birefringence of 4×10^{-4}. Demonstrated performance is excellent for a first fabrication run. Additionally, significant performance advances in HBR-based filters implemented in silica-on silicon have been recently achieved. We will consider said advances in the

next section to demonstrate that high-resolution high-bandwidth polarization-insensitive filters enabling detection of very complex spectral signatures have become a reality.

4. PERFORMANCE ADVANCES.

4.1. High spectral resolution

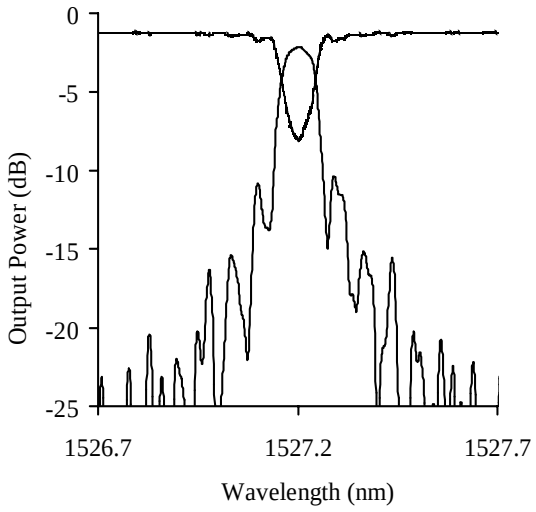

Figure 5. Measured transmission (top line) and reflection (bottom line) of a 20-mm-long non-apodized diffractive structure written in channel waveguide.

Spectral resolution of an HBR-based filter depends on accuracy in feature placement during photolithography as well as refractive index uniformity of layers composing the planar waveguide. If the variations in the optical pathlength caused by either of the above factors are small compared to the resonance wavelength (typically less than tenths of the wavelength), it may be shown that the spectral resolution of a retroreflective HBR is given approximately by

$$\Delta\nu = c/(2\, n_{eff}\, L), \qquad (1)$$

which corresponds to the spectral interval from the peak to first zero in the sinc-function power spectrum of a regular grating of length L. Some spectral signatures require resolution as fine as an Angstrom or less while for others several hundred angstroms is sufficient. Fig. 5 shows the spectrum of a 20-mm-long diffractive structure written in a channel waveguide. The spectral resolution achieved in the structure is better than 0.8 Angstrom corresponding to a coherence length of more that 12 mm. This demonstrated spectral resolution is sufficient to encode vast majority of important spectral signatures.

4.2. Large controlled bandwidth

Total reflective bandwidth of an HBR depends on the reflective strength of individual diffractive elements. This quantity, in turn, is affected by the fraction of mode field amplitude present in the region of the diffractive elements ("confinement factor") and the refractive index contrast between the interfaces forming the diffractive elements. Both these parameters may be adjusted depending on specific application requirements, available materials and process capabilities. Mere increase in the core refractive index increases refractive index contrast at diffractive surfaces and, because of reduced mode size, may also increase the confinement factor. The caveat of such an approach is the accompanying increase in coupling loss at the waveguide to fiber (e.g. SMF28) connection unless special measures are taken to adequately match fiber and waveguide modes.

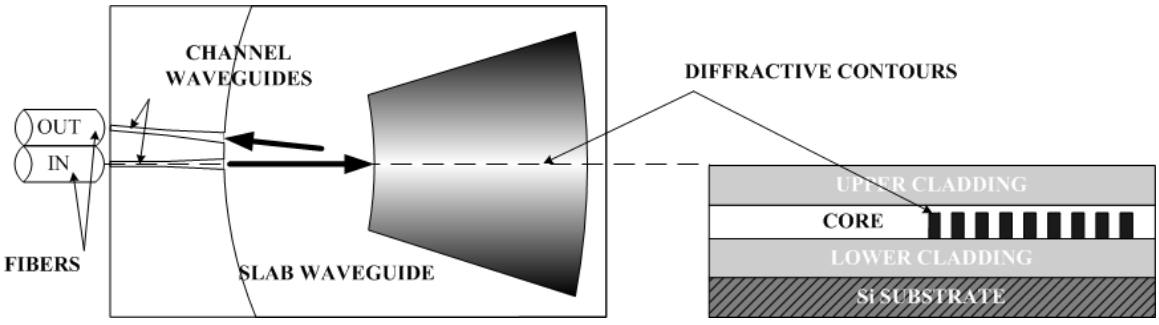

Figure 6. Top view (left) and cross-section (right) of test HBR filter with enhanced reflectivity

We implemented another approach to achieving large reflectivity and wide spectral bandwidth in HBRs comprising the addition of a second guiding layer of higher refractive index (1.49). Diffractive elements are etched into this material. Lower refractive index (1.46) material forms a second guiding layer. In the access channel waveguides (Fig. 6) the higher index layer is stripped. In this way, high refractive index contrast between the element interfaces (0.03 compared to 0.01 employed in the above-discussed spectral comparator) and low fiber-to-waveguide coupling loss (about 1 dB for two interfaces) may be achieved simultaneously. Mode mismatch between the slab region containing the diffractive elements and without diffractive elements is insignificant (estimated at about 0.3 dB). Also special etching procedures were developed to form the diffractive elements with high aspect ratio (Fig. 7). The achieved aspect ratio was1:4 compared to 1:2 employed in the above-discussed spectral comparator. The thickness of the layers was chosen to maximize the mode confinement in the region of the diffractive elements.

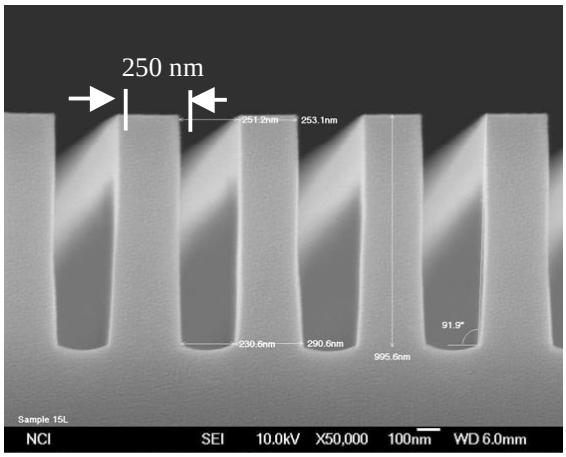

Figure 7. SEM photo of HBR cross-section showing high aspect ratio of the etched diffractive elements.

Using the enhanced architecture, a simple test HBR structure was produced (Fig. 6). It had a layout similar to the one described above with a single input and a single output access channel waveguide. Total length of the HBR was 0.9 mm. The spectral response of the HBR is shown in Fig 8.

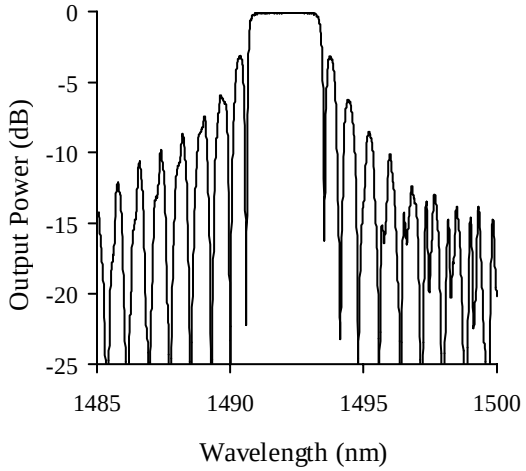

Figure 8. On-chip (excluding coupling to fibers) spectral transfer function of the test filter.

Very high reflectivity of the relatively short structure is evident from the broad passband. The measured FWHM (full width at half maximum) of the passband was 2.8 nm compared to mere 0.75 nm FWHM of weakly reflective 0.9 mm long diffractive structure. The estimated 1/e extinction length (length over with the field of the incident light is

depleted by 1/e) for TE (TM) polarization was 355 μm (375 μm), almost an order of magnitude higher than in the spectral comparator. As evident from the comparison of the extinction lengths for TE and TM, PDL of the resultant structure is negligibly small. PDWL of this and other diffractive structures from the same wafer will be considered later in 4.4.

Using Eq. (1) for the estimate of the reflective bandwidth of an elementary diffractive structure with length of 350 μm, one may found that such extinction length is enabling for HBR-based filter with 200 nm total reflective 3 dB bandwidth for a total physical length of the filter of 20 mm. Combining it with the minimum resolution of 0.1 nm discussed above, we obtain that present performance of HBR-based filter allow to store an astonishing 2000 spectral features in a single 5 x 30 mm HBR chip.

4.3. Small scattering loss

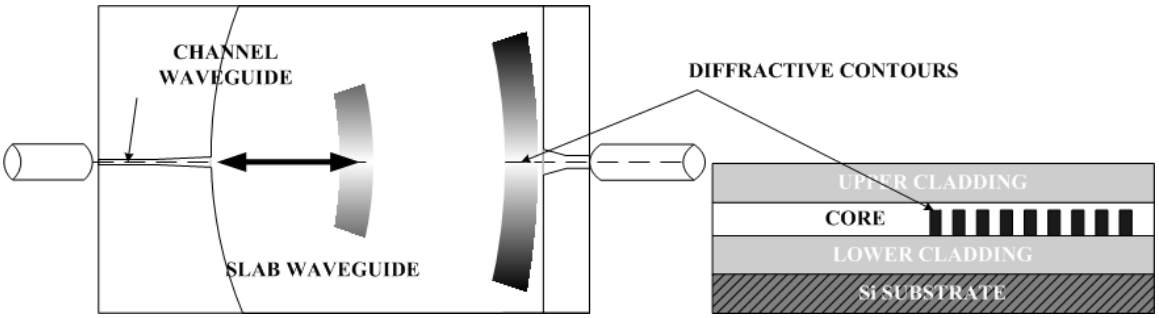

Figure 9. Top view (left) and cross-section (right) of resonance cavity.

Another structure implemented to test the limits of HBR performance is a resonance cavity[5] formed by two confocal HBR mirrors in a concentric Fabry-Pero geometry (Fig. 9). The measured transmission and reflection spectrum of the cavity is shown in Fig. 10. The finesse value of the cavity (ratio of FSR to the transmission bandpass) provides highly accurate indication of intrinsic losses associated with scattering and absorption of light in HBR structures. The measured finesse value of the cavity for TE(TM) polarization was 10.2 (9.2). Comparison to the theoretical finesse values calculated based on 1/e extinction length discussed in 4.2 of 9.4 (8.3) indicates that one round-trip cavity loss is close to zero and upper-limited to 1.8% (1.2%) for TE (TM) input polarization. Thus, propagation and scattering losses within HBR filters have been confirmed to be very small allowing fabrication of low insertion loss power-efficient filters.

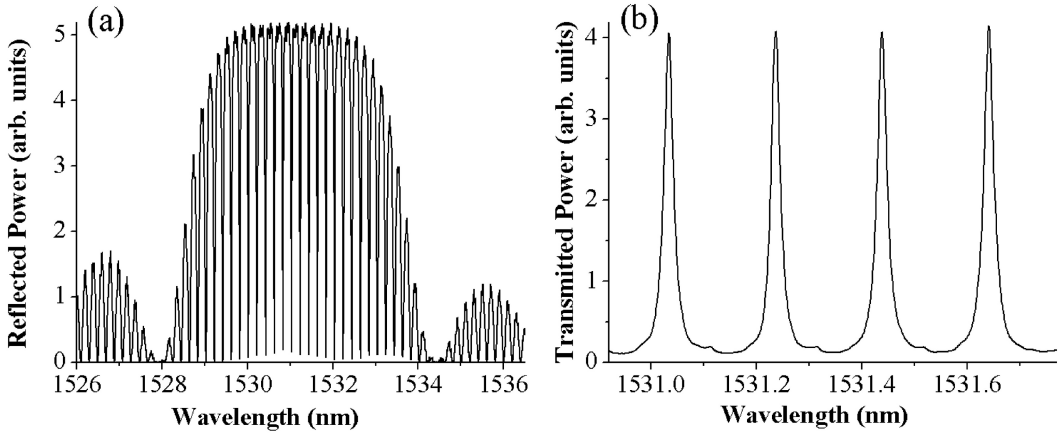

Figure 10. (a) Cavity reflection profile. (b) Transmission spectrum at the center of the HBR passband. Finesse calculated from the spectrum gives an accurate evaluation of scattering and absorption losses.

4.4 Small polarization dependence.

For some spectral recognition applications, independence of the filter spectral response from state of polarization of the input light is an important requirement. We call a filter polarization independent when its output power does not appreciably fluctuate with changes in the input state of polarization ("polarization-dependent loss") and the shift in the filter spectral transfer function with input polarization ("polarization-dependent wavelength shift" or PDWL) is small compared to the spectral feature size. HBR's for the chosen range of refractive index contrast (0.01 to 0.03) were measured to have no appreciable polarization-dependent loss, as discussed in 4.2. PDWL is a common problem of silica-on-silicon planar lightwave circuits and is a result of birefringence originating primarily from thermal-expansion coefficient mismatch of the silicon substrate and silica waveguide layers. Typically this problem is solved for channel waveguides by adjusting dopant contents of the silica uppercladding and balancing stresses experienced by the channel waveguide. We have demonstrated an alternative solution that works for slab waveguides as well as channel waveguides. According to our test results, adjustment in the morphology of the diffractive elements and thicknesses of the layers forming the waveguide may be used to control the birefringence and consequently PDWL. This approach was used in fabrication of the HBR disclosed in 4.2 to achieve PDWL of 80 pm, which is sufficient for most applications and by itself is a great improvement compared to 600 pm polarization-dependent wavelength shift observed in the spectral comparator considered in section 3. Further, it was found that other HBR's produced on the same wafer but having different morphology of the diffractive elements exhibited PDWL ranging from 200 pm to essentially 0 pm (within the accuracy of the measurements which was about 5 pm). Thus we have demonstrated that substantially zero PWDL is achievable using design adjustments for a specific wafer architecture and fabrication parameters.

5. CONCLUSION.

Recent advances in the development of HBR-based filters have demonstrated the feasibility of highly customizable multi-wavelength filters based on photonics nanostructures programmable to recognize spectra containing up to 2000 spectral lines. Such filters rival or exceed performance of free space gratings, thin film filters and Bragg gratings and may be monolithically integrated with detectors in III-V active materials. This new technological platform holds a great promise of being next-generation optical engine for spectral signature recognition for remote sensing, biological, chemical and defense applications. We note that HBRs can be overlain using a variety of techniques offering a pathway of recording whole families of highly complex spectral signatures on a single cm-scale chip.

REFERENCES

1. T. W. Mossberg, "Planar holographic optical processing devices," *Opt. Lett.*, vol.26, no.7, pp. 414-416, 2001.
2. Y. Hibino, "Recent advances in high-density and large-scale AWG multi/demultiplexers with higher index-contrast silica-based PLCs", *IEEE J. Select. Topics Quantum Electron.*, vol. 8, pp. 1090-1101, 2002.
3. T. Erdogan, "Fiber Grating Spectra", *J. Lightwave Technol.*, vol. 15, pp. 1277-1294, 1997.
4. T. W. Mossberg , D. Iazikov and C. Greiner "Planar-waveguide integrated spectral comparator", *J. Opt. Soc.Am. A*, vol.21, no. 6, pp. 1088-1092, 2004.
5. C. M. Greiner, D. Iazikov and T. W. Mossberg, "Low-loss silica-on-silicon Fabry-Perot cavity based on holographic Bragg reflectors", *Opt. Lett.*, vol. 30, no.1, to appear January 2005.